
3D Steerable CNNs: Learning Rotationally Equivariant Features in Volumetric Data

Maurice Weiler*
 University of Amsterdam
 m.weiler@uva.nl

Mario Geiger*
 EPFL
 mario.geiger@epfl.ch

Max Welling
 University of Amsterdam / CIFAR
 m.welling@uva.nl

Wouter Boomsma
 University of Copenhagen
 wb@di.ku.dk

Taco Cohen
 Qualcomm AI Research
 taco.cohen@gmail.com

Abstract

We present a convolutional network that is equivariant to rigid body motions. The model uses scalar-, vector-, and tensor fields over 3D Euclidean space to represent data, and equivariant convolutions to map between such representations. These $SE(3)$ -equivariant convolutions utilize kernels which are parameterized as a linear combination of a complete steerable kernel basis, which is derived in this paper. We prove that equivariant convolutions are the most general equivariant linear maps between fields over \mathbb{R}^3 . Our experimental results confirm the effectiveness of 3D Steerable CNNs for the problem of amino acid propensity prediction and protein structure classification, both of which have inherent $SE(3)$ symmetry.

1 Introduction

Increasingly, machine learning techniques are being applied in the natural sciences. Many problems in this domain, such as the analysis of protein structure, exhibit exact or approximate symmetries. It has long been understood that the equations that define a model or natural law should respect the symmetries of the system under study, and that knowledge of symmetries provides a powerful constraint on the space of admissible models. Indeed, in theoretical physics, this idea is enshrined as a fundamental principle, known as Einstein’s principle of general covariance. Machine learning, which is, like physics, concerned with the induction of predictive models, is no different: our models must respect known symmetries in order to produce physically meaningful results.

A lot of recent work, reviewed in Sec. 2, has focused on the problem of developing equivariant networks, which respect some known symmetry. In this paper, we develop the theory of $SE(3)$ -equivariant networks. This is far from trivial, because $SE(3)$ is both non-commutative and non-compact. Nevertheless, at run-time, all that is required to make a 3D CNN equivariant using our method, is to parameterize its filter kernels as a linear combination of pre-computed steerable basis kernels. Hence, the 3D Steerable CNN incorporates equivariance to symmetry transformations without deviating far from current engineering best practices.

The architectures presented here are examples of Steerable G-CNNs [4, 6, 24, 29], which represent their input as scalar-, vector- and tensor fields over a homogeneous space (\mathbb{R}^3 in this case), and use steerable filters [9, 23] to map between such representations. The convolution kernel is modeled as a tensor field satisfying an equivariance constraint, from which steerable filters arise automatically.

* Equal Contribution. Mario Geiger initiated the project, derived the kernel space constraint and wrote the first network implementation. Maurice Weiler solved the kernel constraint analytically, designed the anti-aliased kernel sampling in discrete space and coded / ran many of the Tetris & CATH experiments.

Source code is available at <https://github.com/mariogeiger/se3cnn>.

We evaluate the 3D Steerable CNN on two challenging problems: prediction of amino acid preferences from atomic environments, and classification of protein structure. We show that a 3D Steerable CNN improves upon state of the art performance on the former task. For the latter task, we introduce a new and challenging dataset, and show that the 3D Steerable CNN consistently outperforms a strong CNN baseline over a wide range of training set sizes.

2 Related Work

There is a rapidly growing body of work on neural networks that are equivariant to some group of symmetries [5, 6, 8, 11, 12, 16, 18–22, 30]. At a high level, these models can be categorized along two axes: the group of symmetries they are equivariant to, and the type of geometrical features they use. The class of regular G-CNNs represents data in terms of scalar fields on a group G (e.g. $SE(3)$) or homogeneous space G/H (e.g. $\mathbb{R}^3 = SE(3)/SO(3)$) [17], whereas steerable (or induced) G-CNNs represent data in terms of more general fields over a homogeneous space [4]. The models described in this paper are of the steerable kind, since they use general fields over \mathbb{R}^3 . Fields can be considered as a formalization of the idea of convolutional capsules [11, 21].

The most closely related works are the Tensor Field Network (TFN) of [24] and the N-Body networks (NBNs) of [15], which were released on ArXiv towards the end of our project. The main differences are as follows: both TFN and NBN work on irregular point clouds, whereas our model works on regular 3D grids. Point clouds are more general, but regular grids can be processed more efficiently. The second difference is that whereas the TFN and NBN use Clebsch-Gordan coefficients to parameterize the network, we simply parameterize the filter bank as a linear combination of steerable basis filters. Clebsch-Gordan coefficient tensors have 6 indices, and depend on various phase and normalization conventions, making them tricky to work with. Our implementation requires only a very minimal change from the conventional 3D CNN.

The two dimensional analog of our work is the harmonic network [29]. Other closely related work includes the regular discrete 3D G-CNNs of [27, 28], which were shown to achieve excellent data efficiency in medical imaging and 3D model recognition problems.

3 SE(3)-Equivariant Networks

Our general approach to building $SE(3)$ -equivariant networks will be as follows: First, we will specify for each layer n a linear *transformation law* $\pi_n(g) : \mathcal{F}_n \rightarrow \mathcal{F}_n$ (also known as a *group representation*), which describes how features in the feature space \mathcal{F}_n (defined below) transform under transformations of the input by $g \in SE(3)$. Then, we will study the vector space of equivariant linear maps (intertwiners) Φ between adjacent feature spaces:

$$\text{Hom}_{SE(3)}(\mathcal{F}_n, \mathcal{F}_{n+1}) = \{\Phi \in \text{Hom}(\mathcal{F}_n, \mathcal{F}_{n+1}) \mid \Phi \pi_n(g) = \pi_{n+1}(g) \Phi, \forall g \in SE(3)\}. \quad (1)$$

Here $\text{Hom}(\mathcal{F}_n, \mathcal{F}_{n+1})$ is the space of linear (not necessarily equivariant) maps from \mathcal{F}_n to \mathcal{F}_{n+1} . By finding a basis for this space and parameterizing layer Φ_n as a linear combination of basis maps, we can make sure that layer $n+1$ transforms according to π_{n+1} if layer n transforms according to π_n , thus guaranteeing equivariance of the whole network by induction.

The feature transformation laws π we consider are the so-called *induced representations*, which describe the motion of scalar-, vector-, tensor- and other kinds of fields [2, 4, 6, 10]. As shown below, equivariant maps between induced representations of $SE(3)$ can always be expressed as convolutions with equivariant / steerable filter banks. The space of equivariant filter banks is a linear subspace of the space of all filter banks. We will show how to find a basis for this space, which can be used to parameterize the filter banks used in the $SE(3)$ -equivariant CNN.

3.1 Fields and their Transformations

A convolutional network produces a stack of K_n feature maps f_k in each layer n . We can model the feature maps as (well-behaved) functions $f_k : \mathbb{R}^3 \rightarrow \mathbb{R}$. Written another way, we have a map $f : \mathbb{R}^3 \rightarrow \mathbb{R}^{K_n}$ that assigns to each position x a feature vector $f(x) \in \mathbb{R}^{K_n}$, which we call the fiber. In practice, f has bounded support, meaning that $f(x) = 0$ outside of some compact domain $\Omega \in \mathbb{R}^3$. So we define \mathcal{F}_n as the vector space of continuous maps from \mathbb{R}^3 to \mathbb{R}^{K_n} with compact support.

In this paper, we impose additional structure on the fibers. Specifically, we assume the fiber consists of a number of geometrical quantities, such as scalars, vectors, and tensors, stacked into a single

K_n -dimensional vector. The assignment of such a geometrical quantity to each point in space is called a *field*. Thus, the feature spaces consist of a number of fields, each of which consists of a number of channels.

What makes a geometrical quantity anything more than an arbitrary grouping of feature channels? The reason that each geometrical quantity is to be considered a single unit, distinct from the others, is that it transforms independently under rigid body motions, whereas its component channels do not do so by themselves. This idea is known as Weyl's principle, and has been proposed as a way of formalizing the notion of disentangling [3, 13].

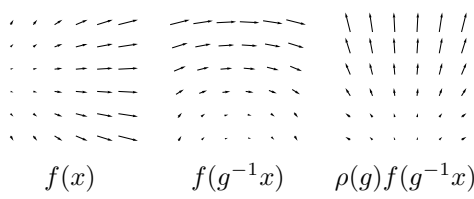


Figure 1: To transform a planar vector field by a 90° rotation g , first move each arrow to its new position, keeping its orientation the same, then rotate the vector itself. This is described by the induced representation $\pi = \text{Ind}_{\text{SO}(2)}^{\text{SE}(2)} \rho$, where $\rho(g)$ is a 2×2 rotation matrix that mixes the two coordinate channels.

contrast, consider the common situation where in the input space we have an RGB image with $K = 3$ channels. Then $f(x) \in \mathbb{R}^3$, and the rotation can be described using the same formula $\rho(r)f(r^{-1}x)$ if we choose $\rho(r) = I_3$ to be the 3×3 identity matrix for all r . Since $\rho(r)$ is diagonal for all r , the channels do not get mixed, and so in geometrical terms, we would describe this feature space as consisting of three scalar fields, *not* a 3D vector field. The RGB channels each have an independent physical meaning, while the x and y coordinate channels of a vector do not. In physics terminology: if we change to a different frame of reference, the coordinates of a vector mix together, while the coordinates of an array of scalars does not.

We have seen two examples of fields, each one determined by a different choice of ρ . As one might guess, there is a one-to-one correspondence between the type of field and the type of group representation ρ . Hence, we can speak of a ρ -field.

So far, we have concentrated on the behaviour of a field under rotations and translations separately. A 3D rigid body motion $g \in \text{SE}(3)$ can always be decomposed into a rotation $r \in \text{SO}(3)$ and a translation $t \in \mathbb{R}^3$, written as $g = tr$. So the transformation law for a ρ -field is given by the formula:

$$[\pi(tr)f](x) = \rho(r)f(r^{-1}(x - t)). \quad (2)$$

The map π is known as the representation of $\text{SE}(3)$ induced by the representation ρ of $\text{SO}(3)$, which is denoted by $\pi = \text{Ind}_{\text{SO}(3)}^{\text{SE}(3)} \rho$.

3.2 Irreducible $\text{SO}(3)$ features

We have seen that there is a correspondence between the type of field and the type of inducing representation ρ , which describes the rotation behaviour of a canonical fiber. To get a better understanding of the space of possible fields, we will now define precisely what it means to be a representation of $\text{SO}(3)$, and show how any such representation can be constructed from elementary building blocks called irreducible representations.

A group representation ρ assigns to each element in the group an invertible $n \times n$ matrix. Here n is the dimension of the representation, which can be any positive integer (or even infinite). For ρ to be called a representation of G , it has to satisfy $\rho(gg') = \rho(g)\rho(g')$, where gg' denotes the composition of two transformations $g, g' \in G$, and $\rho(g)\rho(g')$ denotes matrix multiplication.

To make this more concrete, and to introduce the concept of an irreducible representation, we consider the classical example of a rank-2 tensor (i.e. matrix). A 3×3 matrix A transforms under rotations as $A \mapsto R(r)AR(r)^T$, where $R(r)$ is the 3×3 rotation matrix representation of the abstract group

element $r \in \text{SO}(3)$. This can be written in matrix-vector form using the Kronecker / tensor product: $\text{vec}(A) \mapsto [R(r) \otimes R(r)] \text{vec}(A) \equiv \rho(r) \text{vec}(A)$. This is a 9-dimensional representation of $\text{SO}(3)$.

One can easily verify that the symmetric and anti-symmetric parts of A remain symmetric respectively anti-symmetric under rotations. This splits $\mathbb{R}^{3 \times 3}$ into 6- and 3-dimensional linear subspaces that transform independently. According to Weyl's principle, these may be considered as distinct quantities, even if it is not immediately visible by looking at the coordinates A_{ij} .

The 6-dimensional space can be further broken down, because scalar matrices $A_{ij} = \alpha \delta_{ij}$ (which are invariant under rotation) and traceless symmetric matrices also transform independently. Thus a rank-2 tensor decomposes into representations of dimension 1 (trace), 3 (anti-symmetric part), and 5 (traceless symmetric part). More generally, it can be shown that any representation of $\text{SO}(3)$ can be decomposed into irreducible representations of dimension $2l + 1$, for $l = 0, 1, 2, \dots, \infty$. The irreducible representation acting on this $2l + 1$ dimensional space is known as the Wigner-D matrix of order l , denoted $D^l(r)$.

In representation-theoretic terms, we have reduced the 9-dimensional representation ρ into irreducible representations of dimension 1, 3 and 5. We can write this as

$$\rho(r) = Q^{-1} \left[\bigoplus_{l=0}^2 D^l(r) \right] Q, \quad (3)$$

where we use \bigoplus to denote the construction of a block-diagonal matrix with blocks $D^l(r)$, and Q is a change of basis matrix that extracts the trace, symmetric-traceless and anti-symmetric parts.

Since any $\text{SO}(3)$ representation can be decomposed into irreducibles, we only use irreducible features in our networks. This means that the feature vector $f(x)$ in layer n is a stack of F_n features $f^i(x) \in \mathbb{R}^{2l_i+1}$, so that $K_n = \sum_{i=1}^{F_n} 2l_i + 1$.

3.3 The Space of Equivariant Kernels

A continuous linear map between \mathcal{F}_n and \mathcal{F}_{n+1} can be written using a continuous kernel κ with signature $\kappa : \mathbb{R}^3 \times \mathbb{R}^3 \rightarrow \mathbb{R}^{K_{n+1}} \times \mathbb{R}^{K_n}$, as follows:

$$[\kappa \cdot f](x) = \int_{\mathbb{R}^3} \kappa(x, y) f(y) dy \quad (4)$$

Lemma 3.1. *The map $f \mapsto \kappa \cdot f$ is equivariant if and only if for all $g \in \text{SE}(3)$,*

$$\kappa(gx, gy) = \rho_2(r) \kappa(x, y) \rho_1(r)^{-1}, \quad (5)$$

Proof. For this map to be equivariant, it must satisfy $\kappa \cdot [\pi_1(g)f] = \pi_2(g)[\kappa \cdot f]$. Expanding the left hand side of this constraint, using $g = tr$, and the substitution $y \mapsto gy$, we find:

$$\kappa \cdot [\pi_1(g)f](x) = \int_{\mathbb{R}^3} \kappa(x, gy) \rho_1(r) f(y) dy \quad (6)$$

For the right hand side,

$$\pi_2(g)[\kappa \cdot f](x) = \rho_2(r) \int_{\mathbb{R}^3} \kappa(g^{-1}x, y) f(y) dy. \quad (7)$$

Equating these, and using that the equality has to hold for arbitrary $f \in \mathcal{F}_n$, we conclude:

$$\rho_2(r) \kappa(g^{-1}x, y) = \kappa(x, gy) \rho_1(r). \quad (8)$$

Substitution of $x \mapsto gx$ and right-multiplication by $\rho_1(r)^{-1}$ yields the result. \square

Theorem 3.2. *A linear map from \mathcal{F}_n to \mathcal{F}_{n+1} is equivariant if and only if it is a cross-correlation with a rotation-steerable kernel.*

Proof. Lemma 3.1 implies that we can write κ in terms of a one-argument kernel, since for $g = -x$:

$$\kappa(x, y) = \kappa(0, y - x) \equiv \kappa(y - x). \quad (9)$$

Substituting this into Equation 4, we find

$$[\kappa \cdot f](x) = \int_{\mathbb{R}^3} \kappa(x, y) f(y) dy = \int_{\mathbb{R}^3} \kappa(y - x) f(y) dy = [\kappa \star f](x). \quad (10)$$

Cross-correlation is always translation-equivariant, but Eq. 5 still constrains κ rotationally:

$$\kappa(rx) = \rho_2(r) \kappa(x) \rho_1(r)^{-1}. \quad (11)$$

A kernel satisfying this constraint is called rotation-steerable. \square

We note that $\kappa \star f$ (Eq. 10) is exactly the operation used in a conventional convolutional network, just written in an unconventional form, using a matrix-valued kernel (“propagator”) $\kappa : \mathbb{R}^3 \rightarrow \mathbb{R}^{K_{l+1} \times K_l}$.

Since Eq. 11 is a linear constraint on the correlation kernel κ , the space of equivariant kernels (i.e. those satisfying Eq. 11) forms a vector space. We will now proceed to compute a basis for this space, so that we can parameterize the kernel as a linear combination of basis kernels.

3.3.1 Equivariant Kernel Basis

As mentioned before, we assume that the K_n -dimensional feature vectors $f(x)$ consist of irreducible features $f^i(x)$ of dimension $2l_{in} + 1$. In other words, the representation $\rho_n(r)$ that acts on feature vectors in layer n is block-diagonal, with irreducible representation $D^{l_{in}}(r)$ as the i -th block. This implies that the kernel $\kappa : \mathbb{R}^3 \rightarrow \mathbb{R}^{K_{n+1} \times K_n}$ splits into blocks $\kappa^{jl} : \mathbb{R}^3 \rightarrow \mathbb{R}^{(2j+1) \times (2l+1)}$ which (by Eq. 11) are constrained to transform as

$$\kappa^{jl}(rx) = D^j(r) \kappa^{jl}(x) D^l(r)^{-1}. \quad (12)$$

To bring this constraint into a more manageable form, we vectorize these kernel blocks to $\text{vec}(\kappa^{jl}(x))$, so that we can rewrite the constraint as a matrix-vector equation

$$\text{vec}(\kappa^{jl}(rx)) = (D^l \otimes D^j)(r) \text{vec}(\kappa^{jl}(x)), \quad (13)$$

where we used the orthogonality of D^l . The tensor product of representations is itself a representation, and hence can be decomposed into irreducible representations. For irreducible $\text{SO}(3)$ representations D^j and D^l of order j and l it is well known [10] that $D^j \otimes D^l$ can be decomposed in terms of $2\min(j, l) + 1$ irreducible representations of order¹ $|j - l| \leq J \leq j + l$. That is, we can find a change of basis matrix Q of shape $(2l + 1)(2j + 1) \times (2l + 1)(2j + 1)$ such that the representation becomes block diagonal:

$$[D^l \otimes D^j](r) = Q^T \left[\bigoplus_{J=|j-l|}^{j+l} D^J(r) \right] Q \quad (14)$$

Thus, if we change the basis and solve for $\eta^{jl}(x) = Q \text{vec}(\kappa^{jl}(x))$ instead of $\text{vec}(\kappa^{jl}(x))$, the constraint splits further into constraints of the form $\eta^{jl,J}(rx) = D^J(r) \eta^{jl,J}(x)$ on $2J+1$ dimensional invariant subspaces. This is a famous equation for which the well-known (unique) solution is given by the spherical harmonics $Y^J(x) = (Y_{-J}^J(x), \dots, Y_J^J(x))$. More specifically, since x lives in \mathbb{R}^3 instead of the sphere, the solutions are given by spherical harmonics modulated by an arbitrary continuous radial function $\varphi : \mathbb{R}^+ \rightarrow \mathbb{R}$ as $\eta^{jl,J}(x) = Y^J(x/\|x\|) \varphi(\|x\|)$.

To obtain a complete basis, we can choose a set of basis functions $\varphi^m : \mathbb{R}_+ \rightarrow \mathbb{R}$ for the radial functions, and define basis functions $\eta^{jl,Jm}(x) = Y^J(x/\|x\|) \varphi^m(\|x\|)$. Following [26], we choose a Gaussian profile $\varphi^m(\|x\|) = \exp(-\frac{1}{2}(\|x\| - m)^2/\sigma^2)$ in our implementation. The basis for $j = l = 1$, and a single radial shell, is shown in Fig. 2.

By mapping each $\eta^{jl,Jm}$ back to the original basis via Q^T and unvectorizing, we obtain a basis $\kappa^{jl,Jm}$ for the space of equivariant kernels between features of order j and l . This basis is indexed by the radial index m and frequency index J . In the forward pass, we linearly combine the basis kernels as $\kappa^{jl} = \sum_{Jm} w^{jl,Jm} \kappa^{jl,Jm}$ using learnable weights w , and stack them into a complete kernel κ , which is passed to a standard 3D convolution routine.

¹There is a fascinating analogy with the quantum states of a two particle system for which the angular momentum states decompose in a similar fashion.

²The matrix Q can be expressed in terms of the Clebsch-Gordan coefficients, but this is not necessary here.

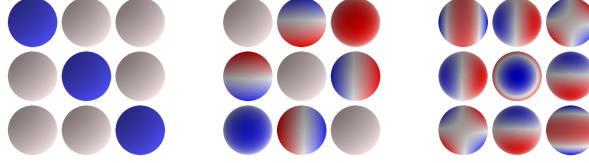


Figure 2: Basis for the space of steerable kernels κ^{jl} (for $j = l = 1$, i.e. 3D vector fields as input and output). From left to right we plot three 3×3 matrices, for $j - l \leq J \leq j + l$ i.e. $J = 0, 1, 2$. The matrices exhibit the trace, anti-symmetric, and symmetric-traceless structure. Each 3×3 matrix corresponds to one learnable parameter per radial basis function φ^m .

3.4 Equivariant Nonlinearities

In order for the whole network to be equivariant, every layer, including the nonlinearities, must be equivariant. In a regular G-CNN, any elementwise nonlinearity will be equivariant because the regular representation acts by permuting the activations. In a steerable G-CNN however, special equivariant nonlinearities are required.

Trivial irreducible features, corresponding to scalar fields, do not transform under rotations. So for these features we use conventional nonlinearities like ReLUs or sigmoids. For higher order features we considered tensor product nonlinearities [15] and norm nonlinearities [29], but settled on a novel gated nonlinearity. For each non-scalar irreducible feature $\kappa_n^i \star f_{n-1}(x) = f_n^i(x) \in \mathbb{R}^{2l_{in}+1}$ in layer n , we produce a scalar gate $\sigma(\gamma_n^i \star f_{n-1}(x))$, where σ denotes the sigmoid function and γ_n^i is another learnable rotation-steerable kernel. Then, we multiply the feature (a non-scalar field) by the gate (a scalar field): $f_n^i(x) \sigma(\gamma_n^i \star f_{n-1}(x))$. Since $\gamma_n^i \star f_{n-1}$ is a scalar, $\sigma(\gamma_n^i \star f_{n-1})$ is a scalar, and multiplying any feature by a scalar is equivariant.

3.5 Discretized Implementation

In a computer implementation of $\text{SE}(3)$ equivariant networks, we need to sample both the fields / feature maps and the kernel on a discrete sampling grid in \mathbb{Z}^3 . Since this could introduce aliasing artifacts, care is required to make sure that high-frequency filters are not sampled on a grid of low spatial resolution. This is particularly important for small radii since near the origin only a small number of pixels is covered per solid angle. In order to prevent from aliasing we hence introduce a radially dependant angular frequency cutoff. Aliasing effect originating from the radial part of the kernel basis are counteracted by choosing a smooth Gaussian radial profile as described above. Below we describe how our implementation works in detail.

3.5.1 Precomputation

Before training, we compute basis kernels $\kappa^{jl,Jm}(x_i)$ sampled on a $s \times s \times s$ cubic grid of points $x_i \in \mathbb{Z}^3$, as follows. For each pair of output and input orders j and l we first sample spherical harmonics Y^J , $|j - l| \leq J \leq j + l$ in a radially independent manner in an array of shape $(2J + 1) \times s \times s \times s$. Then, we transform the spherical harmonics back to the original basis by multiplying by $Q^J \in \mathbb{R}^{(2j+1)(2l+1) \times (2J+1)}$, consisting of $2J + 1$ adjacent columns of Q , and unvectorize the resulting array to $\text{unvec}(Q^J Y^J(x_i))$ which has shape $(2j + 1) \times (2l + 1) \times s \times s \times s$.

The matrix Q itself could be expressed in terms of Clebsch-Gordan coefficients [10], but we find it easier to compute it by numerically solving Eq. 14 for 5 samples of $r \in \text{SO}(3)$.

The radial dependence is introduced by multiplying the cubes with each windowing function φ^m . We use integer means $m = 0, \dots, \lfloor s/2 \rfloor$, and the width a fixed width of $\sigma = 0.6$.

Sampling high-order spherical harmonics will introduce aliasing effects, particularly near the origin. Hence, we introduce a radius-dependent bandlimit J_{\max}^m , and create basis functions only for $|j - l| \leq J \leq J_{\max}^m$. Each basis kernel is scaled to unit norm for effective signal propagation [26]. In total we get $B = \sum_{m=0}^{\lfloor s/2 \rfloor} \sum_{|j-l|}^{J_{\max}^m} 1 \leq (\lfloor s/2 \rfloor + 1)(2 \min(j, l) + 1)$ basis kernels mapping between fields of order j and l , and thus a basis array of shape $B \times (2j + 1) \times (2l + 1) \times s \times s \times s$.

3.5.2 Forward pass

At training time, we linearly combine the basis kernels using learned weights, and stack them together into a full filter bank of shape $K_{n+1} \times K_n \times s \times s \times s$, which is used in a standard convolution

routine. Once the network is trained, we can convert the network to a standard 3D CNN by linearly combining the basis kernels with the learned weights, and storing only the resulting filter bank.

4 Experiments

We performed several experiments to gauge the performance and data efficiency of our model.

4.1 Tetris

In order to confirm the equivariance of our model, we performed a variant of the Tetris experiments reported by [24]. In this experiment, we train the model to classify 8 kinds of Tetris blocks, stored as voxel grids, in a canonical orientation. Then we test on tetris blocks rotated by random multiples of 90 degree rotations. As expected, the 3D Steerable CNN generalizes over rotations and achieves 100% accuracy on the test set. In contrast, a conventional CNN achieves 18% accuracy which corresponds to random guessing of the unseen orientations.

4.2 Amino acid environments

We considered the task of predicting amino acid preferences from the atomic environments, a problem which has been studied by several groups in the last year [1, 25]. Since physical forces are primarily a function of distance, one of the previous studies argued for the use of a concentric grid, investigated strategies for conducting convolutions on such grids, and reported substantial gains when using such convolutions over a standard 3D convolution in a regular grid (0.56 vs 0.50 accuracy) [1].

Since the classification of molecular environments involves the recognition of particular interactions between atoms (e.g. hydrogen bonds), one would expect rotational equivariant convolutions to be more suitable for the extraction of relevant features. We tested this hypothesis by constructing the exact same network as used in the original study, merely replacing the conventional convolutional layers with equivalent 3D steerable convolutional layers. Since the latter use substantially fewer parameters per channel, we chose to use the same number of *fields* as the number of channels in the original model, which still only corresponds to only about half the number of parameters (32.6M vs 61.1M (regular grid), and 75.3M (concentric representation)). Without any alterations to the model and using the same training procedure (apart from adjustment of learning rate and regularization factor), we obtained a test accuracy of 0.58, substantially outperforming the conventional CNN on this task, and also providing an improvement over the state-of-the-art on this problem. Further improvements could presumably be obtained by tuning the hyper-parameters of this model. However, instead, we turned our attention to a related task in protein modelling, which is a completely rotation invariant problem, and which thus represents an even more appropriate test for our model.

4.3 CATH: Protein structure classification

The molecular environments considered in the task above are oriented based on the protein backbone. Similar to standard images, this implies that the images have a natural orientation. For the final experiment, we wished to investigate the performance of our Steerable 3D convolutions on a problem domain with full rotational invariance, i.e. where the images have no inherent orientation. For this purpose, we consider the task of classifying the overall shape of protein structures.

We constructed a new data set, based on the CATH protein structure classification database [7], version 4.2 (see <http://cathdb.info/browse/tree>). The database is a classification hierarchy containing millions of experimentally determined protein domains at different levels of structural detail. For this experiment, we considered the CATH classification-level of "architecture", which splits proteins based on how protein secondary structure elements are organized in three dimensional space. Predicting the architecture from the raw protein structure thus poses a particularly challenging task for the model, which is required to not only detect the secondary structure elements at any orientation in the 3D volume, but also detect how these secondary structures orient themselves relative to one another. We limited ourselves to architectures with at least 500 proteins, which left us with 10 categories. For each of these, we balanced the data set so that all categories are represented by the same number of structures (711), also ensuring that no two proteins within the set have more than 40% sequence identity, and adding the additional constraint that all structures fit within a 5 nm sphere centered around its center of mass. This last constraint was introduced to allow us to represent all proteins within a well-defined grid size, and is only violated by a small fraction of the original

data set. The protein structures themselves were simplified to include only C_α atoms (one atom per amino acid in the backbone), and placed at the center of a 50^3 vx grid, where each voxel spans 0.2nm . The values of the voxels were set to the densities arising from placing a Gaussian at each atom position, with a standard deviation of half the voxel width. Finally, we constructed a 10-fold split of the data. To rule out any overlap between the splits (in addition to the 40% homology reduction), we further introduce a constraint that any two members from different splits are guaranteed to originate from different categories at the "superfamily" level in the CATH hierarchy (the lowest level in the hierarchy), and all splits are guaranteed to have members from all 10 architectures.

We first evaluated a conventional CNN. After a number of preliminary experiments, we converged on a ResNet34-inspired architecture using half as many channels as the original, and global pooling at the end. The final model consists of 15, 878, 764 parameters. For details on the architecture and choice of learning and dropout rates, see the supplementary material.

Following the same ResNet template, we then constructed a 3D Steerable network by replacing each layer by an equivariant version, keeping the number of 3D channels fixed. The channels are allocated such that there is an equal number of fields of order $l = 0, 1, 2, 3$ in each layer except the last, where we only used scalar fields ($l = 0$). This network contains only 143, 560 parameters, more than a factor hundred less than the baseline.

We used the first seven of the ten splits for training, the eighth for validation and the last two for testing. The data set was augmented by randomly rotating the input proteins whenever they were presented to the model during training. Note that due to the rotational equivariance of 3D steerable CNNs only the baseline CNN benefits from rotational data augmentation. We train the models for 100 epochs using the Adam optimizer [14], with an exponential learning rate decay of 0.94 per epoch starting after an initial burn-in phase of 40 epochs.

Despite having 100 times fewer parameters, a comparison between the accuracy on the test set shows a clear benefit to the 3D Steerable CNN on this dataset (Figure 3, leftmost value). We proceeded with an investigation of the dependency of this performance on the size of the dataset by considering reductions of the size of each training split in the dataset by increasing powers of two, maintaining the same network architecture but re-optimizing the regularization parameters of the networks. We found that the proposed model outperforms the baseline even when trained on a fraction of the training set size. The results further demonstrate the accuracy improvements across these reductions to be robust (Figure 3).

5 Conclusion

In this paper we have presented 3D Steerable CNNs, a class of $\text{SE}(3)$ -equivariant networks which represents data in terms of various kinds of fields over \mathbb{R}^3 . We have presented a comprehensive theory of 3D Steerable CNNs, and have proven that convolutions with $\text{SO}(3)$ -steerable filters provide the most general way of mapping between fields in an equivariant manner, thus establishing $\text{SE}(3)$ -equivariant networks as a universal class of architectures. 3D Steerable CNNs require only a minor adaptation to the code of a 3D CNN, and can be converted to a conventional 3D CNN after training. Our results show that 3D Steerable CNNs are indeed equivariant, and that they show excellent accuracy and data efficiency in amino acid propensity prediction and protein structure classification.

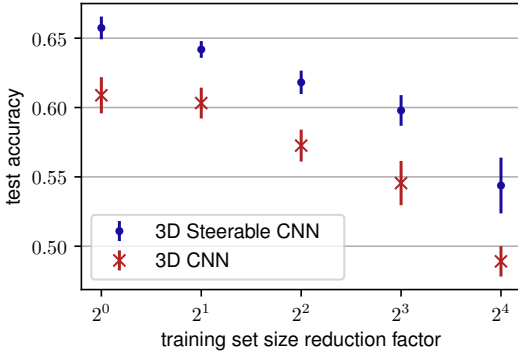


Figure 3: Accuracy on the CATH test set as a function of increasing reduction in training set size.

References

- [1] Wouter Boomsma and Jes Frellsen. Spherical convolutions and their application in molecular modelling. In I Guyon, U V Luxburg, S Bengio, H Wallach, R Fergus, S Vishwanathan, and R Garnett, editors, *Advances in Neural Information Processing Systems 30*, pages 3436–3446. Curran Associates, Inc., 2017.
- [2] T Ceccherini-Silberstein, A Machí, F Scarabotti, and F Tolli. Induced representations and mackey theory. *J. Math. Sci.*, 156(1):11–28, January 2009.
- [3] T Cohen and M Welling. Learning the irreducible representations of commutative lie groups. In *Proceedings of the 31st International Conference on Machine Learning (ICML)*, volume 31, pages 1755–1763, 2014.
- [4] Taco S Cohen, Mario Geiger, and Maurice Weiler. Intertwiners between induced representations (with applications to the theory of equivariant neural networks). March 2018.
- [5] Taco S Cohen and Max Welling. Group equivariant convolutional networks. In *Proceedings of The 33rd International Conference on Machine Learning (ICML)*, volume 48, pages 2990–2999, 2016.
- [6] Taco S Cohen and Max Welling. Steerable CNNs. In *ICLR*, 2017.
- [7] Natalie L Dawson, Tony E Lewis, Sayoni Das, Jonathan G Lees, David Lee, Paul Ashford, Christine A Orengo, and Ian Sillitoe. Cath: an expanded resource to predict protein function through structure and sequence. *Nucleic acids research*, 45(D1):D289–D295, 2016.
- [8] S Dieleman, J De Fauw, and K Kavukcuoglu. Exploiting cyclic symmetry in convolutional neural networks. In *International Conference on Machine Learning (ICML)*, 2016.
- [9] W T Freeman and E H Adelson. The design and use of steerable filters. *IEEE Trans. Pattern Anal. Mach. Intell.*, 13(9):891–906, September 1991.
- [10] David Gurarie. *Symmetries and Laplacians: Introduction to Harmonic Analysis, Group Representations and Applications*. 1992.
- [11] Geoffrey Hinton, Nicholas Frosst, and Sara Sabour. Matrix capsules with EM routing. 2018.
- [12] Emiel Hoogeboom, Jorn W T Peters, Taco S Cohen, and Max Welling. HexaConv. In *International Conference on Learning Representations (ICLR)*, 2018.
- [13] Kenichi Kanatani. *Group-Theoretical Methods in Image Understanding*. Springer-Verlag New York, Inc., Secaucus, NJ, USA, 1990.
- [14] D Kingma and J Ba. Adam: A method for stochastic optimization. In *Proceedings of the International Conference on Learning Representations (ICLR)*, 2015.
- [15] Risi Kondor. N-body networks: a covariant hierarchical neural network architecture for learning atomic potentials. March 2018.
- [16] Risi Kondor, Hy Truong Son, Horace Pan, Brandon Anderson, and Shubhendu Trivedi. Covariant compositional networks for learning graphs. January 2018.
- [17] Risi Kondor and Shubhendu Trivedi. On the generalization of equivariance and convolution in neural networks to the action of compact groups. February 2018.
- [18] Diego Marcos, Michele Volpi, Nikos Komodakis, and Devis Tuia. Rotation equivariant vector field networks. In *International Conference on Computer Vision (ICCV)*, 2017.
- [19] Chris Olah. Groups and group convolutions. <https://colah.github.io/posts/2014-12-Groups-Convolution/>, 2014.
- [20] Siamak Ravanbakhsh, Jeff Schneider, and Barnabas Poczos. Equivariance through Parameter-Sharing. February 2017.

- [21] Sara Sabour, Nicholas Frosst, and Geoffrey E Hinton. Dynamic routing between capsules. In I Guyon, U V Luxburg, S Bengio, H Wallach, R Fergus, S Vishwanathan, and R Garnett, editors, *Advances in Neural Information Processing Systems 30*, pages 3856–3866. Curran Associates, Inc., 2017.
- [22] Laurent Sifre and Stephane Mallat. Rotation, scaling and deformation invariant scattering for texture discrimination. *IEEE conference on Computer Vision and Pattern Recognition (CVPR)*, 2013.
- [23] E P Simoncelli and W T Freeman. The steerable pyramid: a flexible architecture for multi-scale derivative computation. *Proc. Int. Conf. Image Anal. Process.*, 3:444–447, 1995.
- [24] Nathaniel Thomas, Tess Smidt, Steven Kearnes, Lusann Yang, Li Li, Kai Kohlhoff, and Patrick Riley. Tensor field networks: Rotation- and Translation-Equivariant neural networks for 3D point clouds. February 2018.
- [25] Wen Torn and Russ B Altman. 3D deep convolutional neural networks for amino acid environment similarity analysis. *BMC Bioinformatics*, 18(1):302, June 2017.
- [26] Maurice Weiler, Fred A Hamprecht, and Martin Storath. Learning steerable filters for rotation equivariant CNNs. In *Computer Vision and Pattern Recognition (CVPR)*, 2018.
- [27] Marysia Winkels and Taco S Cohen. 3D G-CNNs for pulmonary nodule detection. April 2018.
- [28] Daniel Worrall and Gabriel Brostow. CubeNet: Equivariance to 3D rotation and translation. April 2018.
- [29] Daniel E Worrall, Stephan J Garbin, Daniyar Turmukhambetov, and Gabriel J Brostow. Harmonic networks: Deep translation and rotation equivariance. In *CVPR*, 2017.
- [30] Manzil Zaheer, Satwik Kottur, Siamak Ravanbakhsh, Barnabas Poczos, Ruslan Salakhutdinov, and Alexander Smola. Deep sets. March 2017.

Supplementary Material for “3D Steerable CNNs”

1 Architecture Details for CATH

The baseline 3D CNN architecture for the CATH task was determined through a range of experiments, ultimately converging on a ResNet34-like architecture, with half the number of channels compared to the original implementation (but with an extra spatial dimension), and using a global pooling at the end to obtain translational invariance. After establishing the architecture, we conducted additional experiments to establish good values for the learning and drop-out rates (both in the linear and in the convolutional layers). We settled on a 0.01 dropout rate in the convolutional layers, and L1 and L2 regularization values of 10^{-7} . The final model consists of 15,878,764 parameters.

Following the same ResNet template, we then constructed a 3D Steerable network, by replacing each layer with its equivariant equivalent. In contrast to the model architecture for the amino acid environment, we here opted for a minimal architecture, where we use exactly the same number of *3D channels* as in the baseline model, which leads to a model with the following block structure: $(2, 2, 2, 2), (((2, 2, 2, 2) \times 2) \times 3), (((4, 4, 4, 4) \times 2) \times 4), (((8, 8, 8, 8) \times 2) \times 6), (((16, 16, 16, 16) \times 2) \times 2 + ((256, 0, 0, 0)))$. Here the 4-tuples represent fields of order $l = 0, 1, 2, 3$, respectively. The final block deviates slightly from the rest, since we wish to reduce to a scalar representation prior to the pooling. Optimal regularization settings were found to be a capsule-wide convolutional dropout rate of 0.1, and L1 and L2 regularization values of $10^{-8.5}$. In this minimal setup, the model contains only 143,560 parameters, more than a factor hundred less than the baseline.